Photoneutron strengths in ^{26}Mg at energies of astrophysical interest

R. J. deBoer,* A. Best,† J. Görres, K. Smith, W. Tan, and M. Wiescher
Department of Physics, University of Notre Dame, Notre Dame, Indiana 46556, USA

R. Raut,‡ G. Rusev,§ A. P. Tonchev,‖ and W. Tornow
Department of Physics, Duke University, Durham, North Carolina 27708, USA
and Triangle Universities Nuclear Laboratory, Durham, North Carolina 27708, USA

(Received 11 March 2014; published 23 May 2014)

Background: The ^{22}Ne$(\alpha,n)^{25}$Mg reaction is an important source of neutrons for s-process nucleosynthesis. The neutron production from the reaction is quite sensitive to the low-energy cross section, which is dominated by narrow resonances. The high level density of the ^{26}Mg compound nucleus above the α separation energy prevents simple extrapolations from higher energy and the high Coulomb barrier makes the direct measurements extremely difficult. For this reason, indirect methods must be employed to study the level properties of ^{26}Mg.
Purpose: The current measurement utilizes the reaction ^{26}Mg$(\gamma,n)^{25}$Mg to probe the level structure of the ^{26}Mg compound nucleus from the neutron-separation energy at 11.093 MeV up to $E_x \approx 12$ MeV.
Methods: The High-Intensity γ-ray Source of the Triangle Universities Nuclear Laboratory was used to bombard a ∼16 g sample of enriched ^{26}Mg oxide and the resulting decay neutrons were detected with an array of nine liquid scintillator detectors. Neutron time-of-flight peaks with corresponding energies as low as ∼50 keV were detected. An efficiency measurement of the detectors was made at the University of Notre Dame's nuclear science laboratory to energies as low as 45 keV.
Results: Five resonances were observed at $E_\gamma = 11.150$, 11.289, 11.329, 11.506, and 11.749 MeV and their strengths have been extracted.
Conclusion:. The resulting strengths at $E_\gamma = 11.289$, 11.329, 11.506, and 11.749 MeV are in good agreement with previous measurements. The strength of the resonance at $E_\gamma = 11.150$ MeV is somewhat lower than previously measured but is in reasonable agreement when systematic uncertainties are considered. The results are also consistent with those of ^{25}Mg$(n,\gamma)^{26}$Mg studies where a comparison shows that many of the resonances observed here are the result of multiple unresolved narrow resonances.

DOI: 10.1103/PhysRevC.89.055802 PACS number(s): 26.20.Kn, 27.30.+t

I. INTRODUCTION

The reaction ^{22}Ne$(\alpha,n)^{25}$Mg is primarily responsible for neutron production during helium burning in massive stars ($M \gtrsim 11M_\odot$). This nucleosynthesis environment is identified as the site of the weak s-process where elements above the iron peak, and $A \lesssim 90$, are created (e.g., Ref. [1]). Despite the great desire for a well-known ^{22}Ne$(\alpha,n)^{25}$Mg reaction rate for nucleosynthesis modeling, the experimental challenges of measuring this low-energy cross section have hindered this goal. The chief experimental difficulties are twofold. First, the cross section falls very rapidly at low energies because of the Coulomb repulsion of the two charged entrance channel particles, making direct measurements very difficult with current techniques. Second, the level density of the compound nucleus ^{26}Mg is in an intermediate region where there are enough levels that level identification through indirect techniques is very challenging but not enough levels for a statistical model to be accurate.

The lowest-energy direct measurement is that of Ref. [2], which measured the ^{22}Ne$(\alpha,n)^{25}$Mg cross section down to $E_\alpha \approx 800$ keV, with upper limits extending down to $E_\alpha \approx 600$ keV. This very sensitive measurement, with cross section values in the sub-nanobarn range, just reaches the highest energies important for stellar reaction rate calculations ($E_x = 11.1$ to 11.3 MeV). A strong α-cluster state, i.e., $\theta_\alpha^2 \sim 1$ (where θ_α^2 is the reduced α width), at $E_\alpha = 832(2)$ keV makes a very significant contribution to the stellar rate at helium burning temperatures of ∼0.3 GK. Lower-energy states may also have significant contributions to the rate, especially if they have an α-cluster structure.

The level structure of the ^{26}Mg compound nucleus, just above the α separation energy, has been characterized through indirect techniques. Inelastic proton scattering [3–5], ^{25}Mg$(n,\gamma)^{26}$Mg [6–9], ^{26}Mg$(\gamma,n)^{25}$Mg [10–12], and ^{26}Mg$(\gamma,\gamma')^{26}$Mg [13–15] experiments have been used to measure energies and partial decay widths of levels above the neutron-separation energy $S_n = 11.093$ MeV. Because of the intermediate level density and the limited experimental energy

*Corresponding author: rdeboer1@nd.edu
†Present address: INFN, Laboratori Nazionali del Gran Sasso, 67010 Assergi, Italy.
‡Present address: UGC-DAE Consortium for Scientific Research, Kolkata Centre, Kolkata, India.
§Present address: Los Alamos National Laboratory, Los Alamos, New Mexico, USA.
‖Present address: Lawrence Livermore National Laboratory, Livermore, California, USA.

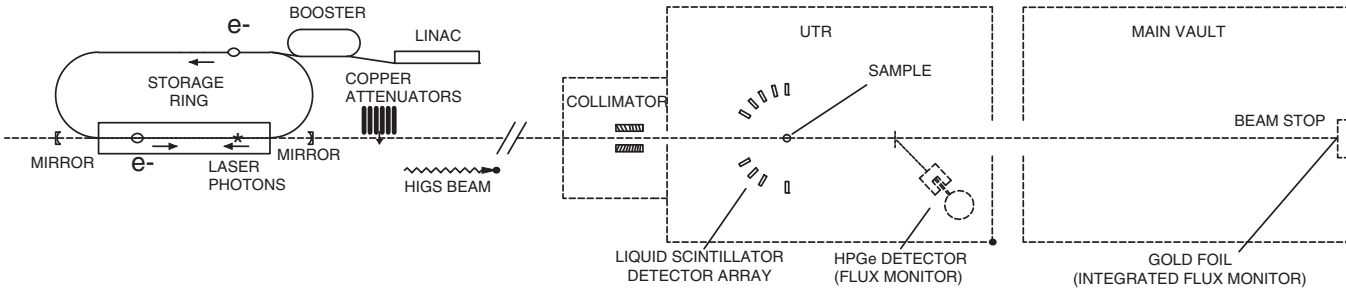

FIG. 1. Layout of the HIγS facility and experimental setup (not to scale). The experiment was preformed in the upstream target room (UTR). The setup shown is for the time-of-flight experiment described in Sec. II B. For the average cross-section measurement described in Sec. II A, the liquid scintillator array is replaced by a ^{3}He counter at the same position on the beam line. The γ beam was allowed to exit the UTR and was stopped in the main vault as this significantly reduced the neutron background level.

resolutions, correspondence of the levels measured using these different techniques has been extremely difficult.

The ^{26}Mg$(\gamma,n)^{25}$Mg measurement of Berman *et al.* (1969) [10] resolved several resonances in the energy region of interest, but further measurements of this type have not been performed since. The same data from this experiment are also presented in Ref. [11]. The astrophysical implications for the ^{22}Ne$(\alpha,n)^{25}$Mg reaction are described in Ref. [10] while Ref. [11] gives more experimental details and presents the results in view of a broader range of (n,γ) studies. Reference [12] gives ^{26}Mg$(\gamma,n)^{25}$Mg measurements with poorer energy resolution.

The measurement of Ref. [10] was the first to observe the level in ^{26}Mg at $E_x = 11.150$ MeV and tentatively assign it a spin of $1^{(-)}$. Several subsequent experiments have attempted to observe this level in the ^{22}Ne$(\alpha,n)^{25}$Mg reaction with no success [2,16–18]. After the attempts using the direct reaction, a ^{26}Mg$(\gamma,\gamma')^{26}$Mg measurement [14] was made which reported a confident spin assignment of 1^+ for this level, determining that it can not be populated in the ^{22}Ne$(\alpha,n)^{25}$Mg reaction. This is consistent with previous ^{26}Mg(p,p') studies which reported the same spin-parity result [3,5]. The goal of the current measurement is to reexamine the level structure using the ^{26}Mg$(\gamma,n)^{25}$Mg reaction as it has only been studied once before.

The measurement has been performed at the High-Intensity γ-ray Source (HIγS) of the Triangle Universities Nuclear Laboratory (TUNL) [19]. First a low-energy-resolution experiment measuring the angle-integrated photoneutron cross section from $E_\gamma = 10.80$ to 12.05 MeV was done. A subsequent higher-energy-resolution time-of-flight (TOF) experiment was then performed to resolve the individual levels of interest. A subsequent measurement at the University of Notre Dame's Nuclear Science Laboratory (NSL) helped to characterize the efficiency properties of the liquid scintillator detectors used at HIγS.

The experiments performed at HIγS are described in Sec. II. The detector efficiency measurements at Notre Dame are described in Sec. III. Strengths extracted from the cross-section measurements are presented in Sec. IV and a comparison is made to recent ^{25}Mg$(n,\gamma)^{26}$Mg data using an R-matrix calculation. Summary remarks are presented in Sec. V.

II. MEASUREMENTS OF ^{26}Mg$(\gamma,n)^{25}$Mg

The measurements of the ^{26}Mg$(\gamma,n)^{25}$Mg photoneutron cross section were performed at TUNL's HIγS facility. A circular polarized γ-ray beam was produced by Compton backscattering of laser photons from relativistic electrons in a storage ring. Electrons were accelerated by a 280-MeV linear accelerator and then further accelerated by a booster synchrotron to energies ranging from 498 to 548 MeV. This resulted in γ-ray beams of energies from $E_\gamma = 10.80$ to 12.05 MeV. A detailed review of the facility can be found in Ref. [19]. A 1-cm-diameter lead collimator, positioned 3.5 m upstream from the sample, was used to define the γ-ray beam size which was incident on the sample. The collimation also defined the energy spread $(\Delta E/E)$ of the beam to be $\sim$200 keV at 11.0 MeV. The experimental setup was constructed in the up-stream target room (UTR) of the HIγS facility. The beam was allowed to pass out of the UTR and into the main vault's beam stop to limit background in the UTR. A layout of the facility and setup is given in Fig. 1.

Two samples were used throughout the experimental runs at the HIγS facility. The primary sample consisted of 16.4185 g of magnesium-oxide (MgO) powder, enriched to 99.41(6)% in ^{26}Mg. This sample also contained 0.41(2)% ^{24}Mg and 0.18(4)% ^{25}Mg. Other impurities were on the order of parts per million. The second sample consisted of 4.3 g of natural MgO (79% ^{24}Mg, 11% ^{25}Mg, and 10% ^{26}Mg). The samples were contained in polycarbonate cylindrical containers with 0.16-cm-thick walls and end caps, with an inner cavity 2.30 cm in diameter and 3.10 cm in length. Further details on the samples may be found in Ref. [14]. Attenuation of the γ beam through the material was corrected for using the methods described in Ref. [20] and was found to be between 5.5 and 8.5% depending on the sample's orientation to the beam.

Since the sample material is not pure ^{26}Mg, background reactions could contaminate the neutron spectrum. This is especially true considering no energy information is obtained from the ^{3}He counter. Impurities in the sample and casing include ^{16,17,18}O, ^{24,25}Mg, and ^{12,13}C. Of these impurity nuclei, only ^{17,18}O, ^{25}Mg, and ^{13}C have the neutron channel open at the γ ray beam energies under investigation. The oxygen in the sample is of natural isotopic abundance giving

the ^{17}O and ^{18}O isotopes abundances of 0.04 and 0.21% and photoneutron thresholds of $E_\gamma = 4.14$ and 8.05 MeV, respectively [21]. Both the ^{17}O(γ,n) and ^{18}O(γ,n) reactions have been measured previously [22]. The measurements show a smoothly varying cross section over the energy range of the present measurements and, when scaled by the relative amount of material in the samples, the expected yields are at most a factor of 1/100 those from the ^{26}Mg(γ,n) reaction. The ^{25}Mg(γ,n) reaction has a threshold of $E_\gamma = 7.3$ MeV [21] and previous measurements of the cross section have been made [23]. When scaled by the relative amount of sample material for the enriched sample of 0.18(4)%, the expected yield is smaller than that of the ^{26}Mg(γ,n) reaction by a factor of 1000. The ^{13}C present in the casing is also of a natural isotopic abundance of 1.1%. When the previously measured cross section [24] is scaled by the relative ratio the expected yield is also a smaller than the ^{26}Mg(γ,n) reaction by a factor of 1000. Therefore, no appreciable background is expected given the sensitivity level of the experiment.

The total beam flux for each run was determined by activating a gold foil placed just in front of the beam stop. The γ ray beam was well collimated and the position of the gold foil was aligned with a laser system to ensure that the flux impinging on the gold foil was the same as that on the sample. The beam flux was determined by measuring the activation of the gold foil by observing the decay resulting from the well-known reaction sequence $^{197}\mathrm{Au}\xrightarrow{(\gamma,n)}{}^{196}\mathrm{Au}\xrightarrow{\mathrm{EC}}{}^{196}\mathrm{Pt}$. Characteristic 355-keV γ rays from the subsequent decays of ^{196}Pt were measured off-line in a shielded γ-ray counting station. The uncertainty on the total flux, including geometric alignment, beam attenuation, and the decay properties of the activation, is estimated to be ~10%. The method is described in detail in Ref. [15].

A. Average cross-section measurement

Two experimental runs were performed at the HIγS facility. The first was a low-energy-resolution average cross-section measurement which was performed to characterize the beam induced neutron background. The detector covered a solid angle of nearly 4π and was constructed of several ^{3}He counters moderated by polyethylene. The setup was positioned symmetrically along the beam axis. Samples were placed at the center of the detector with their cylindrical axis centered along the beam direction. Since the detector only gives counting information, the energy resolution is determined by the energy resolution of the beam (~200 keV). The detector efficiency has been studied extensively [25]. The uncertainty is dominated by the efficiency uncertainty and is ~5%.

Beam-induced background measurements were performed below the neutron-separation energy ($S_n = 11.093$ MeV) at $E_\gamma = 10.0$ MeV. Natural background was measured to be ~3 γ/s and the beam-induced neutron background plus the natural background was measured to be 30(2) neutrons/s. The beam induced background is thought to be mostly from $^{\mathrm{nat}}$Pb(γ,n) reactions in the collimator. At these energies, the $^{\mathrm{nat}}$Pb(γ,n) cross section is rather large (~200 mb) (e.g., Ref. [11]). To decrease the background, cadmium sheets and boron-loaded polyethylene blocks were placed as shielding upstream of the detector. This resulted in a decrease in the total background to 24(2) neutrons/s.

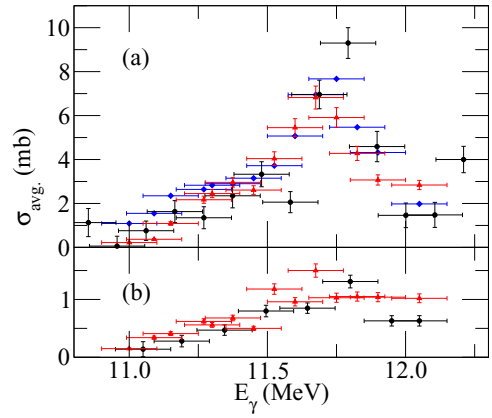

FIG. 2. (Color online) Average cross sections of ^{26}Mg(γ,n) and $^{\mathrm{nat}}$Mg(γ,n). The upper plot (a) shows the ^{26}Mg(γ,n) average cross section while the bottom plot (b) shows the $^{\mathrm{nat}}$Mg(γ,n) average cross section. The data shown in red triangles are from this work while those in black circles are from Ref. [12]. The blue diamond points represent the higher resolution data of Refs. [10,11] convoluted with a 200-keV Gaussian to mimic the resolution of the other measurements.

The energy of the γ-ray beam is determined primarily by the energy of the electrons in the storage ring. The limit of confident energy determination and reproducibility for the facility is ~50 keV. Measurements were therefore made in steps of roughly 50 keV, resulting in cross sections at 15 different beam energies over the range from $E_\gamma = 10.80$ to 12.05 MeV. The count rate was found to be ~1000 neutrons/s, making the observed background quite small in comparison. The resulting average cross section is shown in Fig. 2 compared to a similar measurement made by Ref. [12]. The higher-resolution TOF measurement of Refs. [10,11] is also shown but with the cross section convoluted by a 200-keV Gaussian. All three results are in reasonable agreement.

The structure observed at $E_\gamma = $ ~11.7 MeV can be compared to the higher-energy-resolution spectrum of Refs. [10,11], where it is resolved into three separate resonances: two primary transitions at $E_x = 11.511$ and 11.753 MeV and a secondary transition with strengths of 5.1, 32.5, and 15.0 eV, respectively. Using a Breit-Wigner formalism to characterize the resonance, the strength may be determined by the area of the peak

$$A = 2\pi^2 \lambda\!\!\!^{-2} g_\gamma \frac{\Gamma_{\gamma_0}\Gamma_n}{\Gamma}, \qquad (1)$$

where $\lambda\!\!\!^{-} = \hbar c/2\pi$; $\hbar$ is Planck's constant; $g_\gamma = (2J+1)/2(2J_T+1)$; J is the spin of the excited compound nucleus state; J_T is the intrinsic spin of the target nucleus; and Γ_{γ_0}, Γ_n, and Γ are the ground-state γ-ray, neutron, and total widths, respectively. Since the spin of the resonance is not necessary known, the strength is usually defined as $g_\gamma \frac{\Gamma_{\gamma_0}\Gamma_n}{\Gamma}$. The total strength of the resonance from the present measurement is 56(6) eV, which is in good agreement with the sum of the three underlying resonances given in Ref. [11] of 52.6 eV.

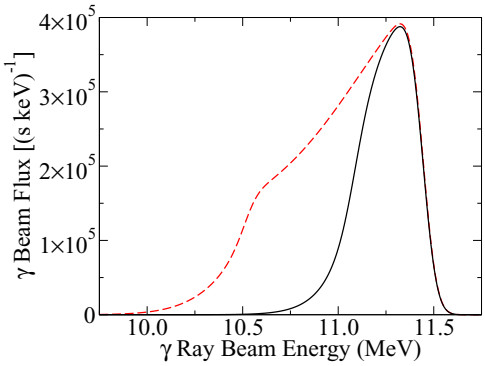

FIG. 3. (Color online) Flux distributions of $E_\gamma = 11.30$ MeV γ-ray beams produced at the HIγS facility. The narrower roughly Gaussian (full width at half maximum ≈200 keV) distribution resulting from the 1-cm collimator is shown by the solid black line. The broader more asymmetric distribution resulting from the 1.9-cm collimator is shown by the dashed red line. The flux distribution is determined by observing the γ beam with a high-purity germanium detector and correcting for detector response as described in Ref. [15] and references therein.

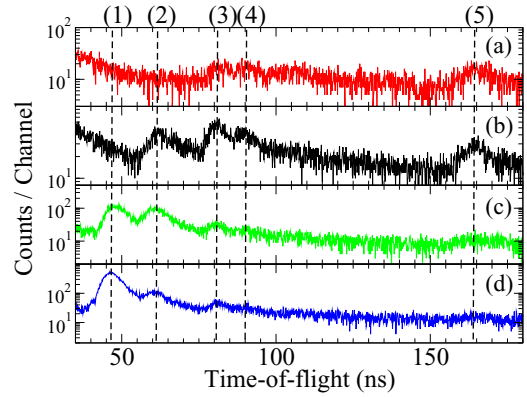

FIG. 4. (Color online) Time-of-flight spectra for a single liquid scintillator detector ($\theta_{lab} = 90^\circ$) at the four beam energies of 11.15 [red (a)], 11.3 [black (b)], 11.5 [green (c)], and 11.8 [blue (d)] MeV. The black dashed lines indicate the centroids of the observed resonances. The neutron energies for the lines labeled (1) through (5) are at $E_n = 637, 397, 227, 188, 55$ keV, which are associated with those seen previously at $E_\gamma = 11.749, 11.506, 11.329, 11.289$, and 11.150 MeV, respectively, by Refs. [10,11].

B. TOF measurements

The second experiment used TOF techniques to obtain better energy resolution in an attempt to resolve individual resonances including the level of interest at $E_x = 11.153$ MeV. Long runs were performed at four beam energies $E_\gamma = 11.15$, 11.30, 11.54, and 11.80 MeV. The neutron TOF was measured relative to the bunching frequency signal from the electron storage ring which had a time between bunches of 179 ns and a duration of less than 1 ns. The collimator for these experimental runs was 3/4″ (1.9 cm) to cover a larger energy range with fewer runs.

The energy distribution of the γ-ray beam was measured at the beginning of each experimental run by placing a 123% high-purity germanium (HPGe) detector directly in the beam (see Fig. 1). Several copper blocks were inserted about 40 m upstream of the detector to reduce the beam intensity so the HPGe detector was not overloaded. The spectrum was corrected for the HPGe detector response [26] to reconstruct the actual energy distribution of the beam. Further details on this method can be found in Refs. [15,27]. The 1.0- and 1.9-cm beam flux distributions, which irradiated the ^{26}Mg sample and the Au foil, are shown in Fig. 3.

The neutron detection setup consisted of nine liquid scintillation detectors. The detectors had an active scintillation volume of 2″ diameter by 2″ length and the scintillation material was of type BC501A. The same two samples, from the previous experiment, of enriched and natural MgO were used but were positioned with their cylindrical axes vertical to the beam so the detectors view of the sample was more symmetric. The detectors were mounted in the horizontal plane 50 ± 3.7 cm from the sample. The distance of 50 ± 3.7 cm was chosen as a compromise between TOF resolution and counting statistics. The TOF resolution at this distance then gives a 10% uncertainty in the energy. The detectors were positioned at backward angles ranging from 90° to 150° (see Fig. 1), where it was found that the beam-induced neutron background was significantly lower than at forward angles.

Neutron TOF peaks are resolved in all nine liquid scintillator detectors, including a low-energy peak corresponding to the ∼50-keV resonance of interest. An example TOF spectrum for the four beam energies is shown in Fig. 4. The different resonance peaks are observed with different intensities in each run reflecting the change in the γ-ray flux (see Fig. 5).

III. EFFICIENCY MEASUREMENTS

To extract the absolute resonance strengths from the TOF measurements at the HIγS facility, the efficiencies of the BC501A liquid scintillator detectors were measured over a

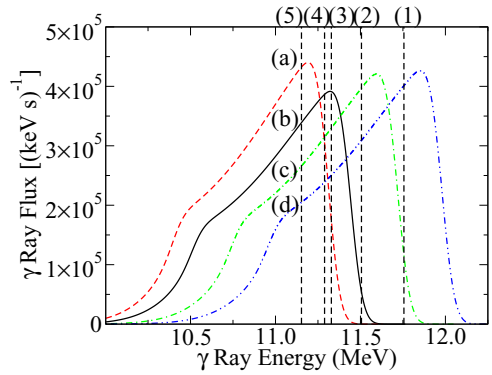

FIG. 5. (Color online) Comparison of the integrated γ-ray fluxes for the four runs at $E_\gamma = 11.15$ (dashed red), 11.30 (black), 11.54 (dot-dashed blue), and 11.8 (dot-dot-dashed blue) MeV. The vertical black dashed lines correspond to the observed resonance energies. The numbered labels correspond to the centroids of the observed resonances and the lettered labels to the flux distributions shown in Fig. 4.

low-neutron-energy range. Since low-energy neutron detection ($E_n \lesssim 100$ keV) is usually not performed with these types of detectors, little information is available in the literature regarding the characteristics of the low energy efficiency. Previously, in Ref. [28], it was observed that the present detectors were sensitive to neutrons at $E_n \approx 90$ keV but efficiency calculations were not performed.

To determine the low energy efficiencies of the liquid scintillator detectors, a calibration measurement was performed at the University of Notre Dame Science Laboratory (NSL) using the well-known cross section of the ^{7}Li$(p,n)^7$Be reaction [29]. Protons were accelerated to energies between $E_p = 1.94$ to 2.9 MeV using the NSL 10-MV Tandem Van de Graaff accelerator. Typical beam currents were ~100 nA. The measurements utilized TOF by bunching the proton beam with a time between bunches of 100 ns and a bunch width of 2 ns.

The ^{7}Li$(p,n)^7$Be threshold is one of the lowest of all stable isotope (p,n) reactions at $E_p = 1.88$ MeV. This insures that neutrons cannot be produced from (p,n) reactions on other sample impurities such as ^{19}F, ^{6}Li, and ^{27}Al, which all have thresholds above $E_p = 4$ MeV. The cross section is also rather large, greater than 1 mb from near threshold up to >3 MeV. The differential cross sections have also been well studied by Ref. [29].

Targets were made by evaporating ^{nat}LiF (92.41(4)% ^{7}Li, 7.59(4)% ^{6}Li) onto thin carbon and thick aluminum backings. Evaporation of the LiF was made at the same time on the carbon and aluminum backings under the same conditions to ensure equal amounts of material were evaporated on both backings. Target thickness were determined by measuring the energy loss of α particles through the LiF target and thin carbon backing. The LiF target thickness was determined to be 23.8(18) μg/cm^2. The uncertainty in the target thicknesses was dominated by stopping power uncertainties and was estimated to be 10%.

The aluminum backings were placed in a special target mounting so they also performed as the pressure cap and beam stop at the end of the evacuated beam pipe. In this way, only the aluminum backing (thickness = 0.82 mm) was between the LiF target material and the detector at 0°. This setup was constructed to prevent significant attenuation of the low-energy neutrons. Attenuation in the air of the target room was negligible.

The detector setup consisted of two detector stations at 0° and 135° relative to the beam direction. These two angles were chosen from the kinematics to measure neutrons over an energy range from ~40 to 1200 keV and to produce the smallest variation in neutron energy over the solid angle range covered by the detectors. The detectors were placed 50 ± 2.5 cm from the LiF target to closely replicate the setup at the HIγS facility. The uncertainty in the distance is dominated by the 2″ thickness of the scintillation detector. The LiF target size was ~5 mm in diameter. Measurements were also made at 75 ± 2.5 cm at 0° and 62 ± 2.5 cm at 135° for each run to positively identify the neutron peak and γ-ray peak from the shift in TOF. An example TOF spectrum is shown in Fig. 6 for ~60-keV neutrons. Test runs were also performed to correct for attenuation of the neutrons from the aluminum beam pipe at 135°.

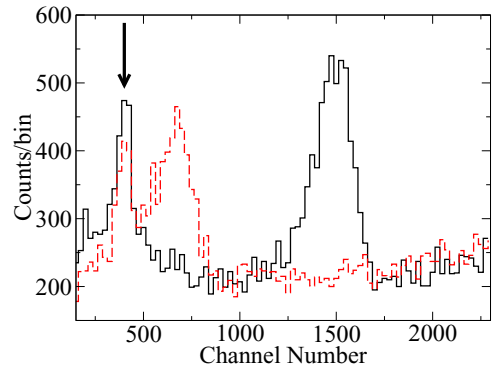

FIG. 6. (Color online) Example TOF spectrum for the liquid scintillator efficiency measurements using the reaction ^{7}Li$(p,n)^7$Be. The spectrum is from a measurement at $E_p = 2.08$ MeV at and angle of $\theta_{lab} = 135°$. The black solid lined histogram is at a distance of 50.0 ± 2.5 cm from the target, the red dashed histogram is at 62.0 ± 2.5 cm. The γ ray peak, indicated by the arrow on the left side of the plot, is in the same position for both runs as expected. The neutron peak shifts according to the difference in TOF. From a calibration with a pulser the conversion from channel number to TOF is 22.8 ns/channel and the shift in the neutron peak is 814 channels, giving a neutron energy of ~59 keV.

The experiment was performed by stepping down in energy from $E_p = 2.9$ to 1.94 MeV. This was done, in part, so special care could be taken to monitor the position of the neutron peak in relation to the prompt γ peak in the neutron TOF spectrum. For each run the peak TOF position was checked against the position calculated from the kinematics of the setup geometry. This was done to monitor for the presence of contaminant peaks. Throughout the experiment no contamination peaks were ever observed.

The uncertainty in the efficiency considers the LiF target thickness (10%), the differential cross section values of Ref. [29] (3 to 27%), and counting statistics (3 to 5%). An example intrinsic efficiency curve is shown in Fig. 7.

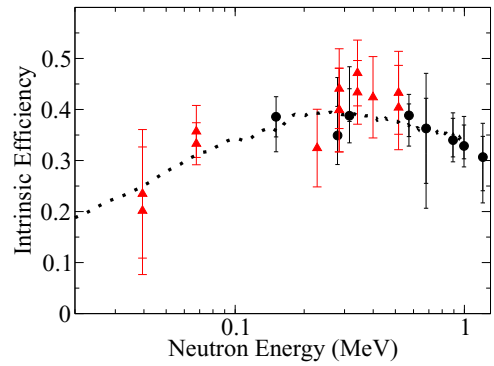

FIG. 7. (Color online) Example efficiency measurements for a BC501A liquid scintillator detector. Measurements made at $\theta_{lab} = 0°$ are shown by black circles, and those made at $\theta_{lab} = 135°$ are shown by red triangles. The dotted line represents a simulation of the efficiency using the code NEFF7 of Ref. [30].

IV. RESULTS AND DISCUSSION

The five resonances from the ^{26}Mg$(\gamma,n)^{25}$Mg reaction shown in Fig. 4 are identified with the five previously observed resonances reported in Refs. [10,11]. The lowest-energy resonance, corresponding to the level in ^{26}Mg at E_x = 11.1535(10) MeV has been observed in the ^{26}Mg$(\gamma,\gamma)^{26}$Mg measurement of Ref. [14].

The efficiency measurements confirm that the liquid scintillation detectors are sensitive to neutrons down to at least E_n = 45 keV. Additional checks were performed during the measurements at HIγS to verify the observation of the lowest-energy resonance: First, the higher-energy resonances were used as references for the TOF calibration. Second, measurements were done with the scintillators at two distances to confirm that the TOF of the peak shifts accordingly. This was done in order to exclude background sources and distinguish from the γ-ray peak.

The higher-energy-resonance structures at E_γ = 11.289, 11.329, 11.506, and 11.749 MeV are used to calibrate the TOF spectra. Contributions to the TOF uncertainty include the uncertainty in the flight path (50 ± 3.7 cm), the beam bunching (179 ± 1 ns), and the statistical uncertainty in the TOF spectrum peak centroids (~2%). This calibration gives the lowest-energy resonance at an excitation energy of E_x = 11.150(8) MeV, in good agreement with the measurements of Ref. [14] of E_x = 11.1535(10) MeV and Ref. [9] of E_x = 11.15336(4) MeV.

A test run was made with one of the detectors moved to a distance of 35 ± 3.7 cm from the target. The resulting TOF spectrum is shown in Fig. 8 compared to the TOF spectrum in the usual running position of 50 ± 3.7 cm. The resonance peaks shift to shorter TOF positions in the closer distance measurement and the resolution becomes poorer. Using the TOF calibration described above, the 50 ± 3.7 cm spectrum should have the neutron peak at 154(11) ns and the 35 ± 3.7 cm peak at 104(11) ns which is consistent with the observed peak positions of 145(3) and 101(5) ns, respectively.

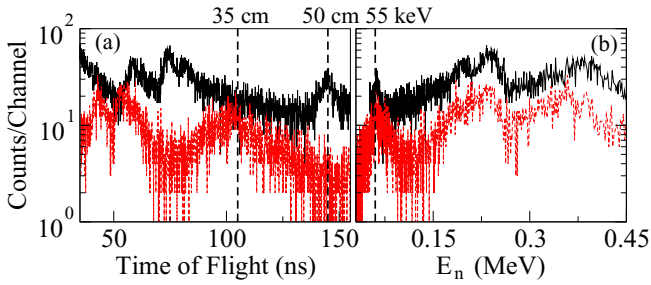

FIG. 8. (Color online) Comparison of two TOF spectra measured at the HIγS facility at the same detection angle but at different distance from the target (upper black solid at 50 ± 3.7 cm, lower red dashed at 35 ± 3.7 cm). Figure 8(a) shows the TOF spectrum. The vertical black dashed lines indicate the location of the E_n = 55 keV neutron peak. The shift in the TOF of the neutron peaks between the two spectra is consistent with the energy calibration. Figure 8(b) shows the spectra where TOF has been converted to energy $\left[E_n = \frac{1}{2} m_n \left(\frac{\Delta d}{\Delta t}\right)^2\right]$ showing good agreement.

TABLE I. Resonance strengths deduced from the current work compared to previous measurements. Uncertainties in the energies are dominated by the 2″ thickness of the scintillation detectors. The systematic uncertainties dominate for the strengths and are chiefly the result of the uncertainty in the beam flux and the detector efficiencies.

E_γ (MeV)	$g_\gamma \frac{\Gamma_{\gamma_0}\Gamma_n}{\Gamma}$ (eV)	
	This work (stat,syst)	Refs. [10,11]
11.150(8)	1.7(0.1,0.5)	2.6(0.3)
11.289(25)	1.01(0.03,0.20)	1.0
11.329(31)	1.59(0.05,0.31)	1.9
11.506(55)	5.7(0.15,1.1)	5.1
11.749(87)	38.9(1.2,7.6)	32.5

The efficiency corrected ^{26}Mg$(\gamma,n)^{25}$Mg yields are found to be isotropic within the uncertainty of the experiment (~10%). The yields are therefore combined for better statistics. The resonance strengths are calculated using Eq. (1). The lowest-energy peak is corrected for self-absorption effects in the sample as described in Ref. [15]. The results for the five observed resonances are given in Table I compared to those of Refs. [10,11].

There is good agreement between our strength measurements and those of Refs. [10,11] for the peaks at E_γ = 11.289, 11.329, 11.506, and 11.749 MeV. The strength of the resonance at E_γ = 11.749 MeV is somewhat higher than that of Refs. [10,11] although still within the systematic uncertainty. This discrepancy is likely the result of a partial contribution from the first excited-state neutron transition which was resolved in Refs. [10,11] but is not in the current experiment.

The strength of the level at E_γ = 11.150 MeV is somewhat smaller than that reported by Refs. [10,11] but is in reasonable agreement considering the large uncertainty associated with the efficiency of the current measurement. The strength for this level can also be calculated using the values of Γ_γ, Γ_n and the spin presented in Ref. [9]. For the γ branching to the ground state Ref. [15] reports $\Gamma_{\gamma_0}/\Gamma_\gamma = 0.7(1)$. The strength is then found to be 3.7(10) eV, which is consistent with the value of 2.6(3) eV of Refs. [10,11] but is much larger than the value found here.

A comparison can also be made with the ^{25}Mg$(n,\gamma)^{26}$Mg measurements of Ref. [9]. These data have considerably better energy resolution than the current experiment but a one-to-one comparison cannot be made since the ^{25}Mg$(n,\gamma)^{26}$Mg data measure the total γ-ray decay channel while the reaction studied here populates only the ground-state γ-ray channel. Even so, for the ground-state decays it is expected that only strong $E1$ and $M1$ transitions will be visible above the level of the background. Since the ground state of ^{26}Mg is $J^\pi = 0^+$, decays from $J^\pi = 1^-$ and 1^+ levels should dominate. Further, for the detailed balance calculation, $\Gamma_{\gamma_{\text{total}}}$ is used for Γ_{γ_0} with the understanding that this will result in an overestimation of the ^{26}Mg$(\gamma_0,n_0)^{25}$Mg cross section. Since the ^{25}Mg$(n,\gamma)^{26}$Mg data only extend up to $E_\gamma - S_n \approx 300$ keV, only the ground-state neutron channel is considered.

Shown in Fig. 9 is a comparison of the ^{26}Mg$(\gamma,n)^{25}$Mg data of Refs. [10,11] to an R-matrix calculation based on

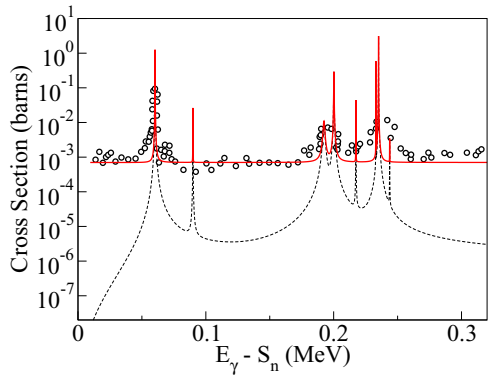

FIG. 9. (Color online) Comparison of the data digitized from Refs. [10,11] with R-matrix calculations based on level parameters from Ref. [9] were Γ_γ has been used for $\Gamma_{\gamma 0}$ for each level. The black dotted line represents the cross section calculated using only the $J = 1$ levels ($E1$ and $M1$ radiation). The red solid line also includes a flat background contribution. It is clear that the resonances observed at $E_\gamma = 11.289$ and 11.329 MeV are the result of multiple unresolved narrow resonances. The higher-energy resonances at $E_\gamma = 11.506$ and 11.749 MeV (not shown) are also likely also the result of more than one level in ^{26}Mg but currently ^{25}Mg$(n,\gamma)^{26}$Mg data is not available in this region.

the SAMMY R-matrix fit to the ^{25}Mg$(n,\gamma)^{26}$Mg data of Ref. [9]. The ^{26}Mg$(\gamma,n)^{25}$Mg data of Refs. [10,11] are used for the comparison instead of the current data since they have better energy resolution and are consistent with current measurement. The R-matrix fit to the ^{25}Mg$(n,\gamma)^{26}$Mg data is used for the comparison instead of the actual data, since those data are never presented as cross sections but instead as yields which retain significant experimental effects.

The comparison shows that two of the resonances observed in the ^{26}Mg$(\gamma,n)^{25}$Mg data at $E_n = 188$ and 227 keV ($E_\gamma = 11.289$ and 11.329 MeV, respectively) correspond to multiple resonances observed in the ^{25}Mg$(n,\gamma)^{26}$Mg data which are designated as single levels of $J^\pi = 1^-$ (see Table III of Ref. [9]). It is also evident that the lowest-energy resonance, corresponding to the 1^+ level at $E_x = 11.15$ MeV, also corresponds to a single resonance in the ^{25}Mg$(n,\gamma)^{26}$Mg data. Besides the $J = 1$ resonances there are several other resonances of higher J reported in Ref. [9]. Several of these have tentative J^π assignments. These other resonances may also make contributions either through strong higher multipolarity transitions or because their tentative spins assignments are incorrect. A comparison of the two resonances observed in the ^{25}Mg$(n,\gamma)^{26}$Mg reaction which are thought to be composed of unresolved resonances observed in the ^{26}Mg$(\gamma,n)^{25}$Mg data are given in Table II.

It is also likely that the broad higher-energy resonances, outside the range of the ^{25}Mg$(n,\gamma)^{26}$Mg data, are also the result of multiple unresolved narrow resonances. Therefore, it should be noted that the resonances observed here and in the previous ^{26}Mg$(\gamma,n)^{25}$Mg data should not be designated as levels in the ^{26}Mg compound nucleus and that higher resolution experiments are needed in order to obtain the unresolved level structure.

TABLE II. Summary of the $J = 1$ resonances observed in the high-energy-resolution ^{25}Mg$(n,\gamma)^{26}$Mg data [9] which are thought to make up the resonances observed in the poorer resolution ^{26}Mg$(\gamma,n)^{25}$Mg measurements of this work and Refs. [10,11]. Contributions from additional resonances may also be significant. Neutron energies from Ref. [9] have been converted to excitation energies using $S_n = 11.09307(4)$ [21].

This work	Ref. [9]			
E_x (MeV)	E_x (MeV)	J^π	Γ_γ (eV)	Γ_n (eV)
11.150(8)	11.15336(4)	1^+	4.1(7)	28(5)
11.289(25)	11.28551(5)	1^-	0.3(3)	1410(60)
	11.29326(4)	(1^-)	1.2(5)	230(20)
11.329(31)	11.31055(4)	(1^-)	4(3)	0.4(2)
	11.32614(4)	(1^-)	6(4)	0.3(2)
	11.32819(5)	(1^-)	3.5(6)	50(20)
	11.32910(4)	(1^-)	2.3(2)	0.5(2)

The results presented here confirm those made previously in Refs. [10,11] for both the resonance energies and strengths. The resolution prevented an improved measurement which was largely the result of the limited TOF path which was necessary in order to get reasonable yields given the amount of sample material and the beam flux ($\sim 3\times 10^8$ γ/s). A significant increase in sample material is possible but the current experiment approaches the limit where attenuation and absorption effects begin to complicate the analysis. Alternatively, the planned HIγS2 facility is expected to have a flux capability of 10^{11} to 10^{12} γ/s. With an increase in flux of a factor of 10^3 to 10^4 over the current measurement, the experiment could be performed with significantly improved TOF resolution. With improved resolution and statistics, anisotropies in the angular distributions may be detectable, which would allow spin assignments to be made. This in turn is extremely helpful when comparing to other measurements like those from the ^{25}Mg$(n,\gamma)^{26}$Mg studies given the level density.

For the indirect study of the ^{22}Ne$(\alpha,n)^{25}$Mg reaction, the energies and strengths verified here help to constrain the level parameters in the ^{26}Mg compound nucleus which are needed to make more confident reaction rate calculations. The other main uncertainty is the α widths of the levels, which the current experiment cannot constrain. The results presented here need to be combined with α width measurements obtained through direct measurements or through transfer reactions like ^{22}Ne$(^6$Li$,d)^{26}$Mg before a reevaluation of the rate is warranted.

V. SUMMARY

Photoneutron cross sections for the reaction ^{26}Mg$(\gamma,n)^{25}$Mg have been measured over an energy range from $E_x = S_n(11.1$ MeV) to 12.05 MeV at the TUNL HIγS facility. The same resonance pattern observed previously in Refs. [10,11] has been observed and the energies have been verified. The strengths of the resonances at $E_\gamma = 11.289$, 11.329, 11.506, and 11.749 are in good agreement with the

previous measurement. For the lowest-energy resonance at $E_x = 11.150$ MeV, the present value of the strength is somewhat lower but still with in the systematic uncertainties. From a comparison with higher resolution ^{25}Mg$(n,\gamma)^{26}$Mg data from Ref. [9] it is likely that the resonances at $E_\gamma = 11.289$ and 11.329 MeV, as well as the higher-energy resonances, are the result several unresolved narrow resonances. Additionally, BC501 material liquid scintillator detectors were found to be sensitive to neutrons as low as $E_n = 45$ keV and their efficiencies were characterized using the well-known ^{7}Li$(p,n)^7$Be reaction.

ACKNOWLEDGMENTS

The authors are grateful to the technical staff of the HIγS facility at TUNL and those of the NSL at Notre Dame. R.J.D. thanks J. H. Kelley, C. W. Arnold, and E. Kwan for their technical support at HIγS and C. Massimi for assistance with the comparisons to the SAMMY fits of ^{25}Mg$(n,\gamma)^{26}$Mg data. This work was funded by the National Science Foundation through Grant No. Phys-0758100, the Joint Institute for Nuclear Astrophysics Grant No. Phys-0822648, and by the U.S. Department of Energy, Office of Nuclear Physics, under Grant No. DE-FG02-97ER41033.

[1] J. José and C. Iliadis, Rep. Prog. Phys. **74**, 096901 (2011).
[2] M. Jaeger, R. Kunz, A. Mayer, J. W. Hammer, G. Staudt, K. L. Kratz, and B. Pfeiffer, Phys. Rev. Lett. **87**, 202501 (2001).
[3] G. M. Crawley, C. Djalali, N. Marty, M. Morlet, A. Willis, N. Anantaraman, B. A. Brown, and A. Galonsky, Phys. Rev. C **39**, 311 (1989).
[4] C. Moss, Nucl. Phys. A **269**, 429 (1976).
[5] A. Tamii, T. Adachi, J. Carter, M. Dozono, H. Fujita, Y. Fujita, K. Hatanaka, H. Hashimoto, T. Kaneda, M. Itoh *et al.*, Nucl. Phys. A **788**, 53 (2007).
[6] H. Weigmann, R. L. Macklin, and J. A. Harvey, Phys. Rev. C **14**, 1328 (1976).
[7] T. A. Walkiewicz, S. Raman, E. T. Jurney, J. W. Starner, and J. E. Lynn, Phys. Rev. C **45**, 1597 (1992).
[8] P. E. Koehler, Phys. Rev. C **66**, 055805 (2002).
[9] C. Massimi, P. Koehler, S. Bisterzo, N. Colonna, R. Gallino, F. Gunsing, F. Käppeler, G. Lorusso, A. Mengoni, M. Pignatari *et al.*, Phys. Rev. C **85**, 044615 (2012).
[10] B. L. Berman, R. L. Van Hemert, and C. D. Bowman, Phys. Rev. Lett. **23**, 386 (1969).
[11] R. J. Baglan, C. D. Bowman, and B. L. Berman, Phys. Rev. C **3**, 672 (1971).
[12] S. C. Fultz, R. A. Alvarez, B. L. Berman, M. A. Kelly, D. R. Lasher, T. W. Phillips, and J. McElhinney, Phys. Rev. C **4**, 149 (1971).
[13] R. Schwengner, A. Wagner, Y. Fujita, G. Rusev, M. Erhard, D. De Frenne, E. Grosse, A. R. Junghans, K. Kosev, and K. D. Schilling, Phys. Rev. C **79**, 037303 (2009).
[14] R. Longland, C. Iliadis, G. Rusev, A. P. Tonchev, R. J. deBoer, J. Görres, and M. Wiescher, Phys. Rev. C **80**, 055803 (2009).
[15] R. J. deBoer, M. Wiescher, J. Görres, R. Longland, C. Iliadis, G. Rusev, and A. P. Tonchev, Phys. Rev. C **82**, 025802 (2010).
[16] V. Harms, K.-L. Kratz, and M. Wiescher, Phys. Rev. C **43**, 2849 (1991).
[17] H. Drotleff, A. Denker, J. Hammer, H. Knee, S. Kchler, D. Streit, C. Rolfs, and H. Trautvetter, Zeitschr. Phys. A Hadrons Nucl. **338**, 367 (1991).
[18] U. Giesen, C. Browne, J. Grres, S. Graff, C. Iliadis, H.-P. Trautvetter, M. Wiescher, W. Harms, K. Kratz, B. Pfeiffer *et al.*, Nucl. Phys. A **561**, 95 (1993).
[19] H. R. Weller, M. W. Ahmed, H. Gao, W. Tornow, Y. K. Wu, M. Gai, and R. Miskimen, Prog. Part. Nucl. Phys. **62**, 257 (2009).
[20] J. H. Hubbell and S. M. Seltzer, Tables of x-ray Mass Attenuation Coefficients and Mass Energy-Absorption coefficients from 1 keV to 20 MeV for Elements Z = 1 to 92 and 48 Additional Substances of Dosimetric Interest (2011), http://www.nist.gov/pml/data/xraycoef/
[21] P. Endt, Nucl. Phys. A **633**, 1 (1998).
[22] J. W. Jury, B. L. Berman, D. D. Faul, P. Meyer, and J. G. Woodworth, Phys. Rev. C **21**, 503 (1980).
[23] R. A. Alvarez, B. L. Berman, D. R. Lasher, T. W. Phillips, and S. C. Fultz, Phys. Rev. C **4**, 1673 (1971).
[24] J. W. Jury, B. L. Berman, D. D. Faul, P. Meyer, K. G. McNeill, and J. G. Woodworth, Phys. Rev. C **19**, 1684 (1979).
[25] C. Arnold, T. Clegg, H. Karwowski, G. Rich, J. Tompkins, and C. Howell, Nucl. Instrum. Methods A **647**, 55 (2011).
[26] S. Carson, C. Iliadis, J. Cesaratto, A. Champagne, L. Downen, M. Ivanovic, J. Kelley, R. Longland, J. R. Newton, G. Rusev *et al.*, Nucl. Instrum. Methods Phys. A **618**, 190 (2010).
[27] G. Rusev, A. P. Tonchev, R. Schwengner, C. Sun, W. Tornow, and Y. K. Wu, Phys. Rev. C **79**, 047601 (2009).
[28] W. Tornow, N. Czakon, C. Howell, A. Hutcheson, J. Kelley, V. Litvinenko, S. Mikhailov, I. Pinayev, G. Weisel, and H. Witaa, Phys. Lett. B **574**, 8 (2003).
[29] C. A. Burke, M. T. Lunnon, and H. W. Lefevre, Phys. Rev. C **10**, 1299 (1974).
[30] G. Dietze and H. Klein, Technical Report, Physikalisch-Technische Bundesanstalt, Braunschweig, Germany, 1982.